Petroleum Research 11 (2026) 761–774

Contents lists available at ScienceDirect

Petroleum Research

journal homepage: http://www.keaipublishing.com/en/journals/petroleum-research/

Full Length Article

Laboratory physical simulation study on water flooding EOR mechanisms and patterns in FM fault- fractured-vuggy reservoirs

Hanmin Tu [a], Jinchuan Wu [a], Zhouhua Wang [a,*], Xingliang Deng [b,c,e], Ping Guo [a], Zhiliang Liu [b,c,d], Haoqi Liao [a]

[a] State Key Laboratory of Oil and Gas Reservoir Geology and Exploitation, Southwest Petroleum University, Chengdu, 610500, China
[b] PetroChina Tarim Oilfield Company, Korla, Xinjiang 841000, China
[c] R&D Center for Ultra Deep Complex Reservoir Exploration and Development, CNPC, Korla, Xinjiang 841000, China
[d] Xinjiang Key Laboratory of Ultra-deep Oil and Gas, Korla, Xinjiang 841000, China
[e] State Energy Key Laboratory for Carbonate Oil and Gas, Korla, Xinjiang 841000, China

ARTICLE INFO

Article history:
Received 12 June 2025
Received in revised form
26 November 2025
Accepted 6 January 2026
Available online 9 January 2026

Keywords:
Fault-fractured-vuggy reservoir
Physical simulation
Enhanced oil recovery
Waterflooding experiment
Water injection parameters
Gravity differentiation

ABSTRACT

The FM fault-fractured-vuggy volatile oil reservoir exhibits significant heterogeneity and rapid production decline. Furthermore, there are notable differences in the effects of depletion development, and the impact of volatile oil degassing on water injection parameters remains unclear. This paper established artificial cores that replicate both single-fractured-vuggy and multi-fractured-vuggy full-diameter systems, reflecting a typical reserves ratio of pores, fractures, and caves in the FM oilfield. Concurrently, water injection experiments were conducted for both single-well and multi-well units after natural energy depletion had occurred. The results indicated favorable development when single-well units opened the lower part of the fracture-vuggy zone, allowing for depletion below bubble pressure at an early stage. Due to dissolved gas flooding at the top of reservoirs, crude oil depletion recovery reached over 67%. The filling of fractures and caves led to delayed degassing: single-phase seepage before degassing was influenced by reservoir physical properties. In contrast, multiphase seepage after degassing was affected by fluid viscosity. The single-well units employed large-volume water injection huff-*n*-puff techniques, resulting in a pronounced gravity oil displacement effect. This method improved cumulative crude oil recovery by more than 5%. Additionally, it was recommended that multi-well units adopt a deep injection and shallow production development strategy, with continuous water flooding enhancing oil recovery by over 40%. However, during the asynchronous injection-production stage, the recovery improvement was limited to only 1%.

© 2026 Chinese Petroleum Society. Publishing services by Elsevier B.V. on behalf of KeAi Communications Co. Ltd. This is an open access article under the CC BY-NC-ND license (http://creativecommons.org/licenses/by-nc-nd/4.0/).

1. Introduction

Carbonate oil and gas resources constitute over 50% of global reserves, highlighting their substantial potential for exploration and development as well as their critical role in the sustainability of oil and gas resources (Chen et al., 2024; Qu et al., 2020; Tian et al., 2019). Fractured-vuggy reservoirs are the primary type of carbonate reservoirs (Ding et al., 2020; Ma et al., 2022b). Recent advancements in " Deep Earth Engineering " have facilitated the discovery of substantial fault-controlled fractured-vuggy oil and gas fields in the Tarim Basin (Ma et al., 2022b), notably the Shunbei and Fuman fields. These reservoirs exhibit significant heterogeneity, with high concentrations of oil and gas reserves located along fault zones. The presence of well-developed dissolution caves and both filled and unfilled fractures further contributes to complex fluid flow patterns, which is governed by a coupled mechanism of percolation and free-phase flow. Oil wells in these reservoirs initially exhibit high production capacities. However, production rates decline rapidly, and development performance varies considerably due to the depletion of natural energy (Jia et al., 2020; Li et al., 2021; Shen et al., 2024; Wang et al., 2016). In 2014, a field water injection trial was implemented in the Fuman oil field, which successfully replenished formation energy and achieved favorable recovery outcomes (Yang et al., 2022). Nevertheless, the complex distribution and connectivity of these

* Corresponding author.
E-mail address: wangzhouhua@126.com (Z. Wang).
Peer review under the responsibility of Editorial Office of Petroleum Research.

https://doi.org/10.1016/j.ptlrs.2026.01.002
2096-2495/© 2026 Chinese Petroleum Society. Publishing services by Elsevier B.V. on behalf of KeAi Communications Co. Ltd. This is an open access article under the CC BY-NC-ND license (http://creativecommons.org/licenses/by-nc-nd/4.0/).

reservoirs present considerable challenges to the scientific understanding of waterflooding strategies in ultra-deep, fault-controlled, fractured-vuggy reservoirs. The mechanisms underlying micro-scale oil displacement and macro-scale oil recovery dynamics remain inadequately understood (Guo et al., 2023; Ma and Duan, 2023).

Physical and numerical simulations are the primary methods employed to evaluate the effectiveness of oil and gas reservoir development (Farhadi et al., 2022; Guo et al., 2019; Ma et al., 2022a; Saw and Mandal, 2023; Zhu et al., 2022a). The seepage mechanisms in ultra-deep, fractured-vuggy, fault-controlled reservoirs are inherently complex, necessitating further refinement of existing theoretical frameworks for numerical simulation. Physical simulations serve a dual role in both mechanism research and flow pattern recognition, providing a foundational basis and validation for seepage behavior in these reservoirs. The physical models utilized for fractured-vuggy reservoirs primarily include full-diameter core models, etched-glass models, and three-dimensional models (Guo et al., 2022; Lu et al., 2022; Wen et al., 2023; Zhao et al., 2020). While etched-glass and three-dimensional models can simulate certain characteristics of reservoir fractures and caves, their sealing limitations generally confine experiments to low-temperature and low-pressure conditions using kerosene. Consequently, these models fail to accurately replicate the actual seepage characteristics under reservoir temperature and pressure conditions, complicating the investigation of the effects of oil degassing on water injection timing and water flooding efficiency. Although full-diameter core experiments can be conducted under reservoir temperature and pressure conditions, they only partially replicate the fractured-vuggy configurations that occur in the reservoir. Therefore, it is essential to develop a high-temperature, high-pressure physical simulation for water flooding in fractured-vuggy reservoirs. This simulation must accurately reflect the reservoir's temperature, pressure, and fluid characteristics. It should also preserve the similarity to the reservoir and the macroscopic configurations of fractures and caves. This advancement will significantly facilitate the study of development methods and mechanisms.

Currently, research on water flooding experiments in fractured-vuggy reservoirs primarily concentrates on the effects of various factors. These factors include the placement of injection-production wells, injection methods, injection rates, and the filling of fractures and caves. The objective of this research is to assess how these factors influence development efficiency and the distribution of residual oil (He et al., 2020; Hou et al., 2016; Hu et al., 2024; Wang et al., 2012, 2014, 2019). He et al. explored the impact of injection-production well placement on development effectiveness using a two-dimensional physical model (He et al., 2020). Their findings indicated that injected water into minor fractures while producing oil from extensive caves, particularly with deep injection and shallow production, favored gravity-driven processes. However, the limitations of temperature, pressure conditions, and model size in two-dimensional experiments hinder the accurate replication of the reservoir's porosity-fracture-vuggy reserve ratio. Additionally, Hou et al. examined water injection methods using a unit from the Tahe oil field (Hou et al., 2016). Their results indicated that pulse water injection, which induces formation pressure imbalances, expanded the sweep volume and significantly improved oil recovery compared to intermittent water injection. Nevertheless, this study primarily focused on multi-well unit water injection methods and did not provide a comparative analysis of the effectiveness of single-well unit water injection. Wang Jing et al. and Wang et al. investigated the influence of filling on water flooding efficiency, suggesting that the extent of pores and caves filling negatively influences the water flooding process (Wang et al., 2014, 2019). Wang Jing et al. employed full-diameter cores to analyze the characteristics of residual oil, concluding that fractured-vuggy structures and injection rates predominantly determine the distribution of residual oil (Wang et al., 2012). However, it is important to note that the experimental oil used was dead oil, which differs from the conditions in actual reservoirs where oil degassing occurs below the bubble point pressure. While these studies emphasized the characteristics of localized fractured-vuggy distributions and strived for precision and complexity, they did not adequately address macroscopic patterns. Moreover, the effect of injection pressure on water flooding efficiency remains unexplored due to the pressure limitations inherent in current two-dimensional and three-dimensional experiments. Additionally, the differences in core and fluid properties under reservoir temperature and pressure conditions have not been adequately explored. Therefore, it is essential to conduct systematic physical simulation studies of water injection development across different development units of fractured-vuggy reservoirs. Such studies should be based on typical fractured-vuggy configuration patterns while taking into account geometric similarity and porosity-fracture-vuggy reserve ratios. This approach will significantly enhance our understanding of the macroscopic aspects of water flooding development in fractured-vuggy reservoirs.

This article presents a comprehensive study of the reservoir characteristics of fault-fractured-vuggy volatile oil reservoirs. Two core models were created, and physical simulation experiments were conducted to investigate the efficacy of water flooding. The study explored the mechanisms of water flooding in both single-well and multi-well units within these reservoirs. Additionally, it proposed suitable water injection methods tailored to the various development units of the reservoirs and elucidated the underlying mechanisms of water flooding.

2. Characteristics of fault-fractured-vuggy volatile oil reservoir

The FM oil field, situated in the Tarim Basin, is classified as a fault-fractured-vuggy reservoir (He et al., 2022; Zhu et al., 2022b). This reservoir is characterized by relatively large oil column heights and a prominent main fault that significantly exceeds the height of the branch faults, thereby facilitating effective vertical connectivity (Fig. 1). The matrix properties of the reservoir are generally suboptimal, with porosity below 5% and permeability under 1mD. However, in certain extensive fractured-vuggy zones, the reservoir properties can markedly improve, with porosity ranging from 10% to 50% and permeability values exceeding 5mD (Wang, 2023; Zhang et al., 2025). The reservoir exhibits extreme heterogeneity, predominantly influenced by fractures and caves. It displays a high density of fractured-vuggy bodies along fault lines, which form strip patterns in the plan view and exhibit “bead-like” structures in the vertical view.

By employing dynamic parameters, well-testing data, and fractured-vuggy structure, the carbonate reservoirs in the FM oil field have been classified into three distinct types: cave-type, pore-vuggy type, and fracture-pore-vuggy type. Currently, 79% of the wells drilled in the FM oil field encounter cave-type reservoirs. These cave spaces are interconnected through fractures of varying orders, which form fractured-vuggy units (Yang et al., 2022). Fractures and caves serve as the fundamental developmental units for fault-fractured-vuggy volatile oil reservoirs. Based on reservoir connectivity, energy status, and development methodologies, fractured-vuggy units are further classified into single-well units utilizing water injection huff-*n*-puff techniques and multi-well units employing continuous water flooding (Wu et al., 2023).

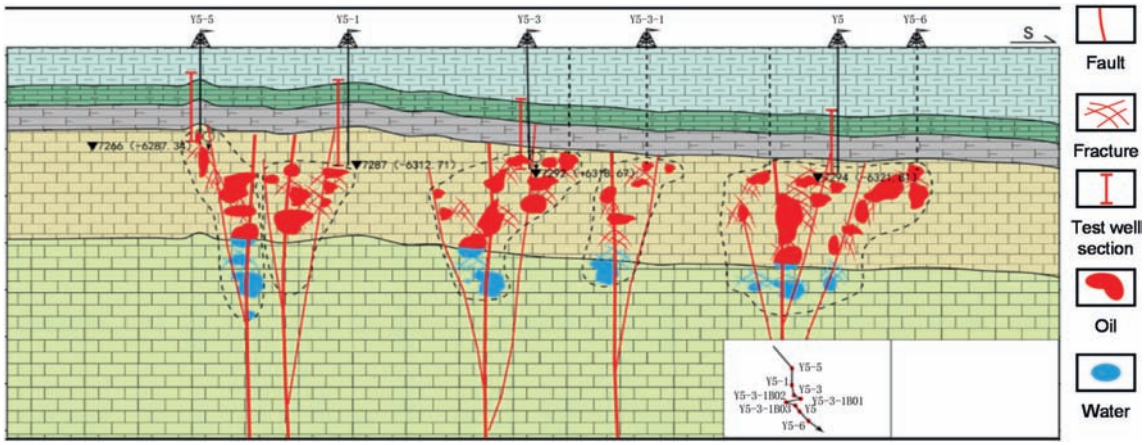


Fig. 1. Schematic diagram of typical reservoir profile (cave reservoirs).

Single-well units initially rely on natural energy for depletion through self-flow production, with energy subsequently supplemented by water injection huff-*n*-puff development. In contrast, the water injection development of multi-well units primarily employs unit water injection to facilitate the lateral or vertical displacement of residual oil between wells during water flooding.

In the FM oil field, temperatures range from 146.93 to 153.86 °C, while pressures vary between 82.35 and 84.82 MPa. The reservoir predominantly consists of light oil and volatile oil, with the latter accounting for 51.7% of the total volume (Wang et al., 2023; Zhang et al., 2015). The average density of the surface oil is 0.82 g/cm^3, accompanied by an average gas-oil ratio (GOR) of 453 m^3/m^3. The saturation pressure of the oil is relatively low, and the reservoir pressure differences range from 38.15 to 68.53 MPa. Furthermore, the oil formation volume factors fluctuate between 1.89 and 2.56, while bubble point pressures range from 32.75 to 40.02 MPa. The contents of intermediate components vary from 14.03% to 25.01%, indicating a generally high level of volatility (Zhu et al., 2020).

According to the *Standard for Reservoir Natural Energy Evaluation Method* (SY/T 6167-1995), the fault-fractured-vuggy reservoir in the FM oil field currently demonstrates a general insufficiency in natural energy. Only 41% of the reservoir is classified as having sufficient or relatively sufficient natural energy, as illustrated in Table 1. In reservoirs identified with insufficient natural energy, poor connectivity is a common issue, marked by a lack of vertical connection between the lower natural water bodies and the upper oil bodies. This disconnection leads to a rapid decline in pressure and production, resulting in challenges such as well abandonment, well plugging, and formation degassing, all of which contribute to a low dynamic recovery factor. A significant amount of residual oil remains trapped between wells and layers, awaiting further exploitation. Water injection has been proven to be an effective method for enhancing oil recovery in such reservoirs by supplementing natural energy and improving overall oil recovery (Lu et al., 2024; Shen et al., 2024).

Table 1
Reservoir natural energy evaluation criteria (SY/T 6167-1995).

Reservoir natural energy classification	Extraction of 1% of the geological reserve stratum pressure drop value, MPa	Elastic production ratio
Enough	<0.2	>30
More adequate	0.2–0.8	8–30
Not enough	0.8–2	2.5–8
Tenuous	>2	<2.5

3. Physical simulation experiment of single/multiple well unit water injection development

3.1. Similarity design

To ensure that physical models accurately represent the actual flow behaviors within the reservoir, their design must adhere to the principles of geometric, kinematic, dynamic, and reserve similarity (Wang et al., 2019; Wen et al., 2023). The similarity design was performed by integrating the cross-sectional profile of the fault-fractured-vuggy reservoir units in the FM oil field (see Fig. 2) with production data, focusing on reservoir dimensions, fluid properties, and production pressure differentials.

Through dimensional analysis and an examination of the characteristics of oil-water flow, similarity criteria for fractured-vuggy reservoirs were established, as detailed in Table 2 (Yang et al., 2020). The similarity index is defined as the ratio of the similarity criteria obtained by substituting the prototype and model parameters into the relevant formula. A similarity index approaching 1 signifies a higher degree of similarity between the

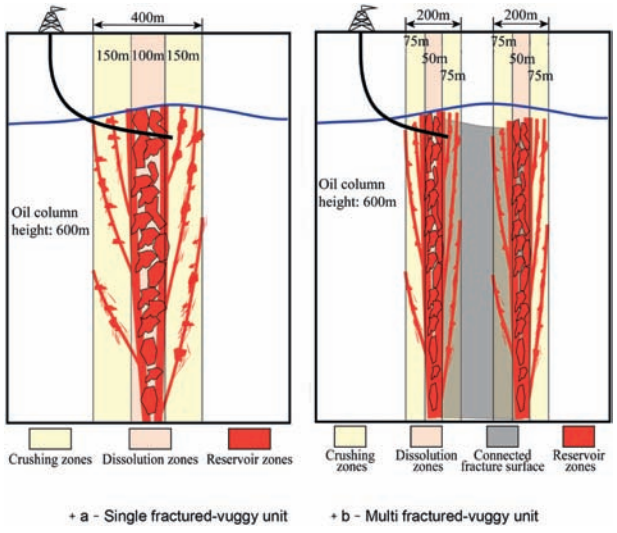


Fig. 2. Schematic diagram of single fractured-vuggy unit section and multi fractured-vuggy unit section.

Table 2
Similarity criteria for fractured-vuggy reservoirs.

Similarity criteria	Physical meaning	Application
d/r	Ratio of vuggy diameter to well-controlled reservoir diameter	Geometric similarity
B/r	Ratio of fracture diameter to well-controlled reservoir diameter	
$\Delta p/\rho_o gl$	Ratio of injection pressure to gravity	Dynamic similarity
$\rho ul/\mu$	Ratio of kinematic inertial force to viscous force	
$Q/(r^2u)$	Ratio of extracted volume to injected volume	Motion similarity
Qt/Qc、Qt/Q_f	Ratio of injection volume to caves or fractures storage volume	Reserve similarity

physical model and the actual reservoir. Consequently, the physical model parameters were meticulously designed to optimize geometric, property, and dynamic similarity. As presented in Table 3, these parameters were calculated to achieve a similarity index as close to 1 as possible.

3.2. Experimental materials

3.2.1. Fluid samples

Based on the PVT data of the original formation fluids from a typical well in the FM oil field and in accordance with *the Standard Method for Analysis of Reservoir Fluid Properties* (GB/T 26981-2020), formation oil samples were prepared using degassed oil and gas obtained from wellhead separators. These samples were conditioned under the original formation pressure of 84.1 MPa and a temperature of 150.3 °C, with a gas-oil ratio of 498 m^3/m^3.

The prepared formation crude oil exhibited a measured bubble pressure of 37.0 MPa, a density of 0.5 g/cm^3, and a viscosity of 0.4 mPa s. The single-degassed gas-oil ratio was determined to be 502 m^3/m^3, which closely matched the properties of the original fluid. The composition of the formation crude oil comprised 67.4 mol% methane (C_1) and 10.4 mol% heavy hydrocarbons (C_{7+}), with specific details outlined in Table 4. To ensure fluid compatibility, the injection water utilized in the experiment was formulated to replicate the formation water, with a total salinity of 7057.82 mg/L, a viscosity of 1.00 mPa s, and classified as $CaCl_2$ type water.

3.2.2. Core samples

Based on the cross-sectional diagram of typical fractured-vuggy bodies in the FM oilfield and an analysis of the vuggy volumes, conceptual models of the reservoir type were developed and digitized. The core design schemes considered the geometric similarity of fractures and the proportional distribution of porosity, fractures, and caves.

Table 3
Physical model parameter design based on similarity criterion.

Parameter	Reservoir	Physical model
Well-controlled diameter	400 m	10 cm
Reservoir height	600 m	15 cm
Width of a main fracture zone	32 m	0.8 cm
Trunk vuggy diameter	160 m	4 cm
Width of a branch fracture zone	8 m	0.2 cm
Branch vuggy diameter	60 m	1.5 cm
Crude oil viscosity	0.4 mPa s	0.4 mPa s
Crude oil density	0.5 g/cm^3	0.5 g/cm^3
Injection rate	200–600 m^3/d	0.125 ml/min
Gravitational acceleration	9.8 m/s^2	9.8 m/s^2

Table 4
Stratigraphic crude oil composition.

Components	Composition (mol%)	Components	Composition (mol%)
N_2	1.8	nC_4	2.1
CO_2	2.7	iC_5	1.0
C_1	67.4	nC_5	1.5
C_2	5.2	C_6	3.8
C_3	3.1	C_{7+}	10.4
iC_4	1.0		

The single-fractured-vuggy core design consists of a primary fracture and multiple branch fractures, with caves interconnected through both the primary and branch fractures. In contrast, the multi-fractured-vuggy core design incorporates two primary fractures and several branch fractures. One primary fracture is located at the top of the core and is connected externally, while the other terminates as a "blind end" at the top. Additionally, three high-angle connecting fractures were designed to link the two primary fractures. The dimensions of the primary and branch fractures are presented in Table 3, with a depth of 20 mm. The connecting fractures have a width of 1 mm, a depth of 20 mm, and an inclination angle of 65°.

The digital models were imported into a computer numerical control (CNC) machine, which employed full-diameter core fracture carving technology to engrave the cores. This process resulted in the preparation of a typical fault-fractured-vuggy core, distinguished by reliable fractured-vuggy configurations and appropriate reservoir proportions. The actual carved cores are illustrated in Fig. 3(a) and (b).

To ensure structural integrity, polytetrafluoroethylene (PTFE) sheets were placed at the bonding surfaces of the carved caves. The cores were then bonded with epoxy resin at elevated temperatures and cooled for a subsequent preparation period. Table 5 shows the porosity and permeability parameters under low-pressure conditions for both the matrix cores and the carved cores. Notably, the relative error between the calculated and measured porosities was found to be less than 3%, indicating that no inadvertent fractures occurred at the bonding interface. In addition, during the experiments, the core was wrapped with a high-temperature, high-pressure PTFE sleeve and subjected to confining pressure to maintain sealing and coupling under reservoir conditions. In addition, the calculated volumes of fractures and vugs were obtained automatically by the engraving machine and compared with the digital model volumes to ensure the accuracy of the carving. The measured values were obtained through gas measurement experiments before and after core engraving, following the Chinese National Standard GB/T 29172-2012 *Core Analysis Method*. After filling, the core parameters were measured again using the same method once the sealing integrity was verified. Specifically, porosity was determined using Boyle's law with helium gas, and permeability was measured using a gas method with nitrogen.

The carved cores measured 5 cm in radius and 15 cm in length. The prepared cores were filled with rock debris of mesh sizes 10–14 and 16–20 combined in a 1:1 mass ratio. Images of the filled cores are presented in Fig. 3(c) and (d). The porosity and permeability parameters under low-pressure conditions for both the single-fractured-vuggy and multi-fractured-vuggy filling cores are detailed in Table 5.

3.3. Experiment apparatus

The experimental apparatus primarily comprises an injection system, a high-temperature and high-pressure full-diameter core

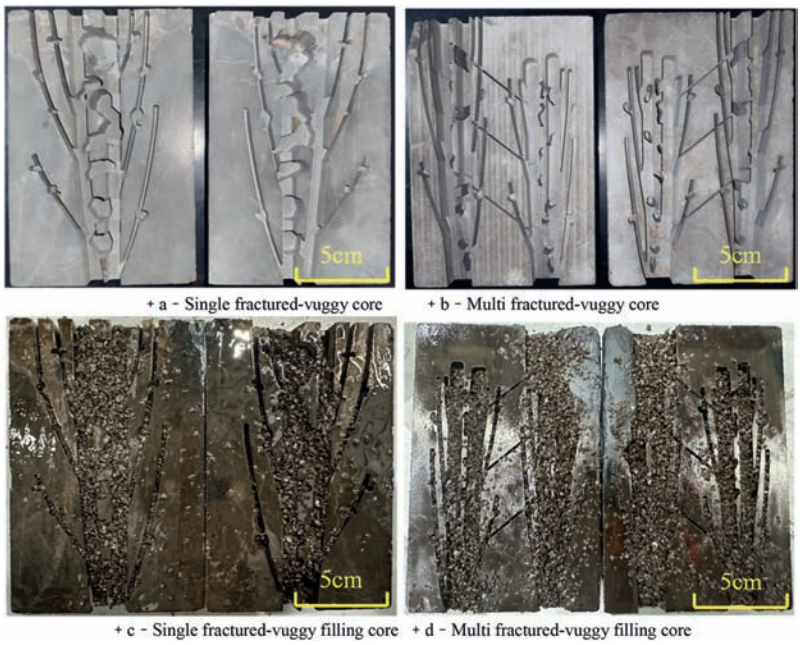


Fig. 3. Physical view of engraved core.

Table 5
Porosity and permeability parameters under a low-pressure condition of matrix cores and post-engraving cores.

Core	Measured values of matrix cores			Calculated value of trunk fractures		Calculated value of trunk caves		Calculated value of branch fractures		Calculated value of branch caves		Calculated value of ϕ (%)	Measured value of ϕ (%)	Measured value of K (mD)	Measured values after filling	
	ϕ (%)	V_ϕ (cm^3)	K (mD)	V_ϕ (cm^3)	ϕ (%)	V_ϕ (cm^3)	ϕ (%)	V_ϕ (cm^3)	ϕ (%)	V_ϕ (cm^3)	ϕ (%)				ϕ (%)	K (mD)
Single fractured-vuggy	2.7	31.3	0.8	47.6	4.0	32.6	2.8	17.7	1.5	2.2	0.2	11.2	11.2	927.0	5.6	61.2
Multi fractured-vuggy	3.1	36.3	0.7	57.4	4.9	23.7	2.0	18.7	1.6	1.0	0.1	11.7	12.0	833.8	5.8	59.6

holder, a temperature and pressure control system, and a production system (see Fig. 4). The core is oriented vertically within the core holder, with the upper and lower sections representing the top and bottom of the reservoir, respectively.

During the experiment, the positions of the injection and production systems are adjusted as necessary to accommodate the differing injection and production methods employed by single-well units and multiple-well units in accordance with the experimental injection-production relationship. The core holder, intermediate vessel, and pressure pumps are designed to withstand maximum temperature and pressure of 200 °C and 200 MPa, respectively. The pressure pumps are capable of achieving an injection speed accuracy of 0.001 ml/s, while the gas meter operates with an accuracy of 1 ml.

3.4. Experimental plans and procedures

To reproduce reservoir conditions, we set the temperature of the entire experimental system, including both the injection system and the core holder, at 150.3 °C. To reproduce reservoir conditions, we set the temperature of the entire experimental system, including both the injection system and the core holder, at 150.3 °C. The core holder is oriented vertically to represent the upper and lower boundaries of the reservoir, simulating the development modes and injection-production relationships that occur during water injection in actual fault-fractured-vuggy reservoirs. Tables 6 and 7 detail the experimental designs for both single-well units and multiple-well units. The experimental pressures shown in Tables 6 and 7 were selected based on different research objectives and also with consideration of the capacity of field injection equipment. The overall experimental design consists of 11 sets, with 7 sets designated for water injection development experiments involving single-well units and 4 sets for multiple-well units.

In the context of single-well units, the experimental cores are categorized into three types: single-fractured-vuggy, multiple-fractured-vuggy, and single-fractured-vuggy filling cores. In Table 6, case 1-1 to case 1–3 were designed to simulate pressure-maintenance production. For these cases, the injection timing and production pressure were set at 1.2 Pb (43.6 MPa), while the injection pressure was raised to 1.5 Pb (54 MPa). By contrast, case 1–4 to case 1–6 used an injection timing and production pressure of 0.5 Pb (18 MPa). This was done to examine how injection timing affects recovery and to study reservoir behavior below the bubble point. In addition, case 1–7 applied an injection pressure of 1.8 Pb (65 MPa) in order to evaluate the influence of injection volume.

In the experiments involving multiple-well units, the process of continuous water flooding following natural energy depletion is simulated, culminating in asynchronous injection and production. Case 2-1 to case 2–4 are designed to investigate the differences in development mechanisms and effects across various reservoir types, injection locations, and timings of water injection.

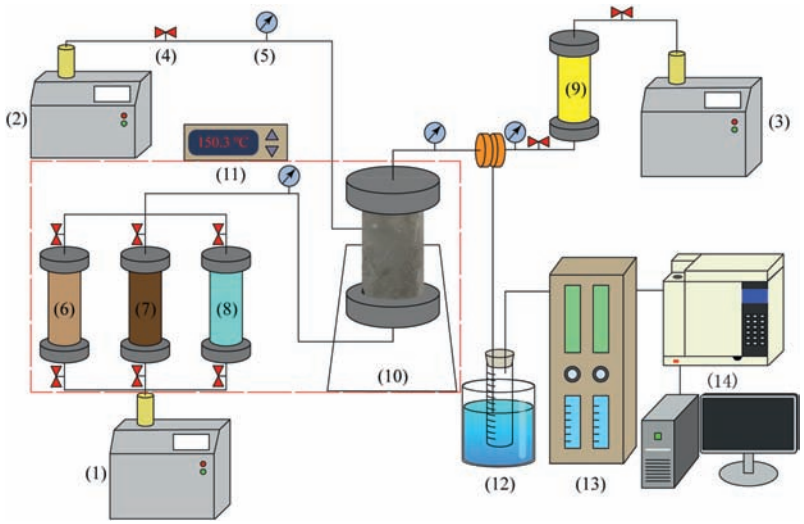


Fig. 4. Schematic diagram of the preferred experimental setup for the water injection development method in seam-hole type reservoirs: (1) Displacement pump, (2) Confining pressure pump, (3) Back pressure pump, (4) Valve, (5) Pressure gauge, (6) Formation crude oil, (7) Degassed crude oil, (8) Formation water, (9) Nitrogen, (10) Core holder, (11) Temperature control system, (12) Gas-liquid separation device, (13) Gas meter, (14) Chromatograph.

Table 6
Typical fault-fractured-vuggy single-well unit water huff-*n*-puff experimental design.

Case	Core type	Depletion process	Water huff-*n*-puff process				Experimental purpose
			Injection timings	Placement of injection and production	Water injection pressurization level	Production pressure	
1–1	Single fractured-vuggy	shallow production	1.2 Pb 43.6 MPa	shallow injection shallow production	1.5 Pb 54 MPa	1.2 Pb 43.6 MPa	comparison of different reservoir types
1–2	Multi fractured-vuggy						
1–3	Single fractured-vuggy filling						
1–4	Single fractured-vuggy	deep production	0.5 Pb 18 MPa	shallow injection shallow production	1.5 Pb 54 MPa	0.5 Pb 18 MPa	comparison of different reservoir types
1–5	Multi fractured-vuggy						comparison of different injection timings
1–6	Single fractured-vuggy filling						comparison of different well locations

Specifically, the timings of water injections are represented by 1.2 Pb and 0.5 Pb, which correspond to injections occurring above and below the bubble pressure, respectively. Furthermore, the water injection pressure levels of 1.5 Pb and 1.8 Pb are employed to simulate varying injection volumes under conditions of high-multiplication water injection. The experimental studies, based on the single and multiple well water injection development parameters outlined in Tables 6 and 7, are performed as follows:

Establishment of Original Formation Conditions: The core is placed in the core holder and subjected to a vacuum for 8 h. Subsequently, the system is heated to 150.3 °C, and degassed crude oil is injected into the core to establish a pressure of 84.05 MPa. The degassed crude oil is then replaced with the prepared formation crude oil. The restoration of original conditions is considered complete when the gas-oil ratio at the outlet stabilizes and aligns with the sample ratio.

Depletion of Natural Reservoir Energy: For single or multiple well units, the top or bottom of the core is opened to facilitate natural energy depletion until the target pressure, as defined in the experimental design (1.2 Pb or 0.5 Pb), is reached. Throughout this process, the volumes of gas and oil produced are measured.

Water Injection Development Experiment: Follow the procedure outlined in Table 6 to conduct single-well unit water injection cycle tests. Start by opening the simulated reservoir top and injecting water to increase the pressure to the target level (1.5 Pb or 1.8 Pb). Allow the well to soak for a designated period, then record the time taken to reach oil-water separation equilibrium. After this, the simulated reservoir top is opened, and production is depleted to the target pressure (1.2 Pb or 0.5 Pb). Complete one cycle of water injection and production, measuring the volumes of gas and oil produced throughout the process. Continue the water injection cycle until no additional oil is produced.

For multiple-well units, continuous water flooding and asynchronous injection-production experiments are performed as outlined in Table 7. Depending on the experimental design, the simulated reservoir is initiated by injecting water either from the bottom (deep injection) or the top (shallow injection), with a gradual increase in water pressure to 1.5 Pb. Continuous water flooding is performed from the designated injection point until no oil is observed at the outlet end (located opposite the water injection point). This observation signifies the conclusion of the continuous water flooding phase.

Table 7
Experimental design of physical simulation for water injection development of multi-fractured-vuggy multi-well unit.

Case	Core type	Depletion process	Continuous water drive process			Asynchronous injection-production process			Experimental purpose
			Injection timings	Placement of injection and production	Experimental purpose	Placement of injection and production	Cycle 1 injection stop pressure	Injection volumes after cycle 1	
2–1	Multi Fractured-vuggy	shallow production	1.2 Pb 43.6 MPa	deep injection shallow production	1.5 Pb 54 MPa	deep injection shallow production	1.8 Pb	production volume of the previous cycle	comparison of different reservoir types
2–2	Multi Fractured-vuggy Filling	shallow production	1.2 Pb 43.6 MPa	deep injection shallow production	1.5 Pb 54 MPa	deep injection shallow production	1.8 Pb	production volume of the previous cycle	
2–3		shallow production	0.5 Pb 18 MPa	deep injection shallow production	1.5 Pb 54 MPa	deep injection shallow production	1.8 Pb	production volume of the previous cycle	comparison of different injection timings
2–4		shallow production	1.2 Pb 43.6 MPa	shallow injection deep production	1.5 Pb 54 MPa	shallow injection deep production	1.8 Pb	production volume of the previous cycle	comparison of different injection locations

Following the asynchronous injection-production design, close the production end and open the injection end, increasing the water pressure to 1.8 Pb. Allow the well to soak while recording the equilibrium time. Subsequently, open the production end, and the well will be depleted to the target pressure of 1.5 Pb, thereby completing a cycle of asynchronous injection production and documenting the experimental data. The water injection volume for the next cycle should equal the total oil and water produced in the previous cycle. This process should be repeated at least three times or until no additional oil is produced.

4. Results and discussion

4.1. Natural depletion development modes and mechanisms

4.1.1. Effect of reservoir type and well placement on depletion development

The development of fault-fractured-vuggy volatile oil reservoirs generally proceeds in two stages: natural depletion followed by water injection. Experimental comparisons highlight how reservoir type and well placement affect depletion performance. During the depletion stage, the cumulative oil recoveries for the single fractured-vuggy core within a single-well unit were 15.1% and 67.2% for shallow and deep productions, respectively. In comparison, the multiple fractured-vuggy core under similar production conditions yielded recoveries of 13.6% and 73.3%. Conversely, within the multiple-well unit containing multiple fractured-vuggy cores, the cumulative oil recovery during the shallow production stage was 14.0%, as depicted in Fig. 5. The experimental results indicate that when depletion reached 1.2 Pb, the recoveries for the single fractured-vuggy core were slightly higher than those for the multiple fractured-vuggy core, with a marginal difference of approximately 1.5%.

Above the bubble point (Pb), flow remained single-phase. Oil recovery was controlled mainly by reservoir connectivity and permeability. The single fractured-vuggy core, which demonstrated enhanced overall connectivity and superior permeability, experienced reduced flow resistance, leading to slightly greater oil recovery compared to the multiple fractured-vuggy core. Well placement had little influence at this stage, with recovery differing by less than 1% between top and bottom production.

Below the bubble point, however, distinct behaviors emerged. In multiple fractured-vuggy cores, a “blind end” at the top

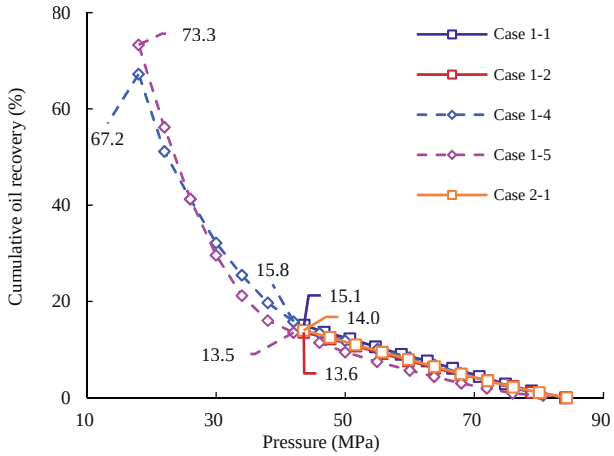


Fig. 5. Comparison of the cumulative oil recovery with pressure during the depletion stage.

facilitated accumulation of released gas, forming a secondary gas cap that strengthened the dissolved gas drive. This process leads to a more efficient dissolved gas drive compared to the single-well unit with a single fractured-vuggy core. When depletion reaches 0.5 Pb, the oil recovery for the multiple fractured-vuggy core is 73.3%, which represents a 6.1% increase over the recovery rate of the single fractured-vuggy core.

In the depletion development of fault-fractured-vuggy volatile oil reservoirs, the gas-oil ratio initially increases but subsequently decreases as pressure declines. This behavior contrasts with that observed in conventional reservoirs, where the gas-oil ratio consistently increases with decreasing pressure. The observed phenomenon can be primarily attributed to the formation of a secondary gas cap at the top of the reservoir when the pressure drops below the bubble point, which enhances the effectiveness of the dissolved gas drive. As additional oil is extracted, the gas-oil ratio decreases to approximately 200 m^3/m^3, as illustrated in Fig. 6.

4.1.2. Effect of fractured-vuggy filling on depletion development

The filling of fractures and caves within the core results in a reservoir that behaves similarly to a porous core with increased permeability. In contrast to unfilled fractured-vuggy cores, the

interactions among various fluids, as well as between liquids and solids during flow, become more critical. Comparative experiments (cases 1-1 vs. 1–3, 1–4 vs. 1–6, and 2-1 vs. 2-2) demonstrate these effects (Fig. 7).

In filled fractured-vuggy cores, the incorporation of filling material not only enhances the reservoir's overall connectivity but also introduces additional complexities in fluid flow dynamics. The enhanced permeability of these filled cores promotes more efficient oil migration. However, the interactions between fluids and the solid matrix become more pronounced, which may impact the efficiency of the natural depletion process.

As shown in Fig. 7, the experimental results highlight the influence of these interactions on oil recovery. In cases where cores are filled, the cumulative oil recoveries during the depletion stage are generally greater than that observed in unfilled cores. This increase is attributed to enhanced connectivity and a more uniform fluid distribution. However, the extent of recovery enhancement varies based on the specific characteristics of the filling material and the reservoirs.

During the depletion stage above the bubble pressure, the extraction process is primarily influenced by the physical properties of the reservoirs. Oil recovery in unfilled cores is approximately 1.5%, 1.9%, and 2.1% higher than that in filled cores for shallow production in the single-well unit with single fractured-vuggy, deep production in the single-well unit with single fractured-vuggy and shallow production in the multi-well unit with multiple fractured-vuggy, respectively. This indicates that the filling of fractures and caves has a negligible impact on oil recovery during this depletion stage. Previous studies investigating the effects of porous media on oil phase behavior have demonstrated that a reduction in pore throat radius leads to an increase in capillary forces, resulting in a more pronounced influence of the porous medium on oil phase behavior (Zou and Gu, 2024). Furthermore, as natural depletion progresses below the bubble pressure, filled cores exhibit reduced porosity and permeability compared to unfilled cores, along with smaller pore throat radii and increased tortuosity. Following the degassing of oil, the time required for the separation of oil and gas is extended, leading to a pronounced degassing delay, which is characterized as a non-equilibrium phenomenon.

The non-equilibrium effect is further substantiated by the gas-oil ratio versus pressure curves observed during the depletion stage, as shown in Fig. 8. Below the bubble pressure, the gas-oil ratio in the filled cores consistently exceeds that in the unfilled core under identical pressure conditions. This observation suggests that the degassing of oil in filled cores is delayed, resulting in a reduction in oil viscosity and an enhancement in fluidity. Consequently, the flow of oil is primarily governed by the properties of the fluid. When the depletion pressure reaches 0.5 Pb, the ultimate recovery of oil in the filled core attains 74.0%, which is 6.8% higher than that in the unfilled core.

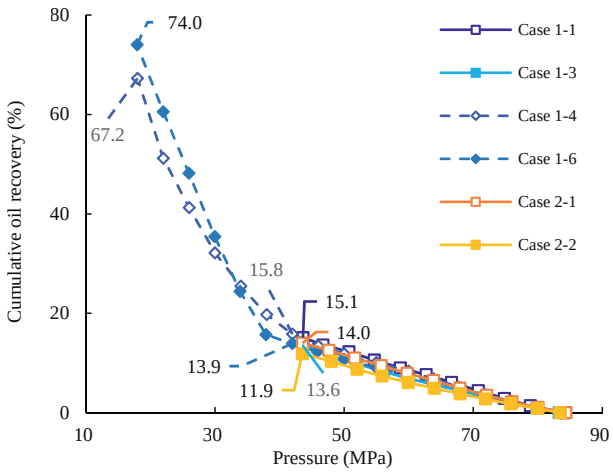


Fig. 7. Comparison of the cumulative oil recovery with pressure during the depletion stage.

These findings highlight the dual role of fracture-vuggy filling: while it exerts minimal impact above the bubble point, it enhances oil recovery below the bubble point by prolonging the effectiveness of dissolved gas drive. This underscores the importance of accounting for filling effects when designing depletion strategies in fractured-vuggy reservoirs.

4.2. Single well unit water huff-n-puff development method and mechanism

In a single-well unit, each water injection cycle includes three stages: injection, soaking, and production. After natural depletion lowers the reservoir pressure, water is injected from the top of the core to restore pressure. During soaking, gravity segregation displaces oil upward. Once equilibrium is reached, oil accumulates at

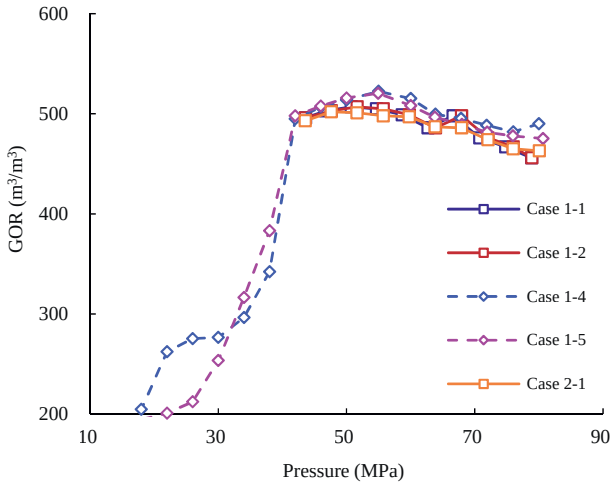


Fig. 6. Comparison of gas-oil ratio with pressure in the depletion stage of different well locations.

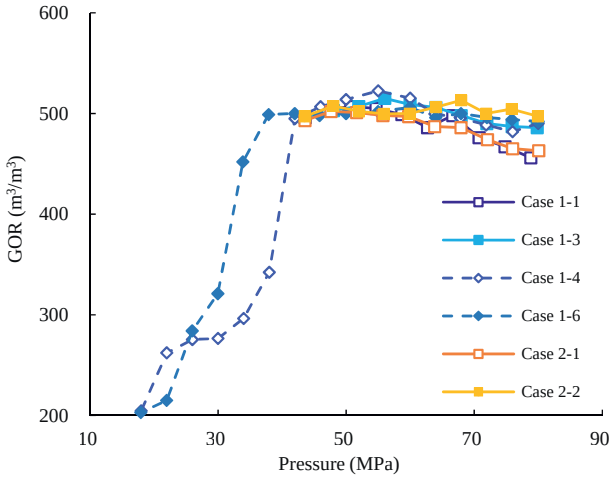


Fig. 8. Comparison of the gas-oil ratio with pressure during the depletion stage.

the top and is produced under the applied pressure differential. Repeated cycles gradually increase overall recovery.

4.2.1. Effect of injection timing on single well unit water huff-n-puff

Fig. 9 shows the variation in cumulative oil recovery and gas-oil ratio during four cycles of water huff-*n*-puff for single fractured-vuggy and multiple fractured-vuggy cores under different injection timings. For the single fractured-vuggy core, cumulative recovery increased by about 5% after four cycles, with little difference between injections above or below the bubble point. In contrast, the multiple fractured-vuggy core performed much better when injection started below the bubble point (0.5 Pb), achieving 11.8% additional recovery, which presents a 7.2% increase compared to the recovery at 1.2 Pb.

When natural energy depletion falls below the bubble point pressure, the initial round of water injection from the top of the core to restore formation energy requires an extended period for the equilibrium segregation of oil, gas, and water to be established. As the injected water displaces oil and gas, these fluids accumulate in the upper section of the core. At this stage, the secondary gas cap has not yet completely dissolved into the oil. Upon initiating production from the top of the core, a substantial volume of secondary gas cap gas is extracted, resulting in a first-round gas-oil ratio of 3940 m^3/m^3, which is markedly higher than the original formation fluid gas-oil ratio of 502 m^3/m^3, as depicted in Fig. 9. As subsequent water injection cycles progress, the extraction of hydrocarbon fluids increases, thereby reducing the time required for fluid equilibrium segregation within the core. Although the gas-oil ratio of the extracted fluid declines, it remains elevated compared to the original formation fluid gas-oil ratio. During the final round of water huff-*n*-puff, the remaining oil volume in the core diminishes, resulting in an increase in the gas-oil ratio of the extracted fluid. Consequently, the driving energy for oil extraction can be attributed to three primary factors: the dissolved gas drive, the elastic expansion of the oil itself, and the elastic expansion energy of the injected formation water. The presence of the "blind end" at the top of the multiple fractured-vuggy core enhances the effect of the dissolved gas drive during the water huff-*n*-puff process, culminating in an 11.8% increase in oil recovery after four cycles.

When the formation pressure exceeds the bubble pressure, the core consists solely of a single oil phase. Once sufficient oil-water segregation equilibrium is achieved, the extraction of oil is primarily governed by the physical properties of the reservoir. The gas-oil ratio of the extracted fluid closely resembles that of the initial formation fluid. The driving energy for extraction includes both elastic expansion of the oil and the elastic expansion effect of the injected water. Therefore, it is advisable to facilitate natural energy depletion below the bubble pressure by opening the bottoms of the fractures. This approach aims to maximize the utilization of the dissolved gas drive for enhanced oil recovery before initiating the water huff-*n*-puff operation.

4.2.2. Effect of water injection volume on single well unit water huff-n-puff

A comparison between case 1–2 and case 1–7 highlights the influence of varying water injection volumes on multiple fractured-vuggy cores following natural energy depletion above the bubble pressure. Water was injected to compensate for this depletion and restore the formation pressure to 1.5 Pb and 1.8 Pb, respectively. Fig. 10 shows the volumes of water injected and the corresponding oil recovery during the water huff-*n*-puff stage.

The findings indicate that an increase in the restored formation pressure correlates with a proportional rise in the volume of water injected, resulting in enhanced oil recovery during the water huff-*n*-puff stage, where oil recovery is defined as the amount of oil extracted during this stage. When the pressure was elevated to 1.8 Pb, the cumulative oil recovery during the water huff-*n*-puff stage reached 7.7%, which is 3.2% higher than the recovery observed at 1.5 Pb. The cumulative water injection volumes required for pressurization to 1.8 Pb and 1.5 Pb were 56.0 ml and 34.2 ml, respectively, corresponding to approximately 0.4 HCPV and 0.2 HCPV (Hydrocarbon Pore Volume).

The substantial volume of water injection, characterized by elevated pressure, provides a more robust driving force that enhances the pressure gradient within the core. This process facilitates communication between the two principal trunk fractures and caves of the multi-fractured-vuggy core. Additionally, it propels water into regions with reduced permeability, expanding the contact area between oil and water during water flooding. This expansion enhances the movement of greater quantities of crude oil. However, in the low-permeability area, incomplete contact and separation of oil and water can prolong the equilibrium separation time. In the short term, cumulative oil recovery increased, after which the growth leveled off. Following the initial two cycles of water huff-*n*-puff at a higher pressurization level of 1.8 Pb, the cumulative oil recoveries were recorded at 6.4% and 7.5%, respectively. The recovery rates in the third and fourth cycles tended to stabilize at around 7.7% (Fig. 10). In contrast, the pressurization level of 1.5 Pb, which involved a lower injection volume, resulted in a more uniform distribution of the injected water within the reservoir. This led to a gradual and consistent growth in the

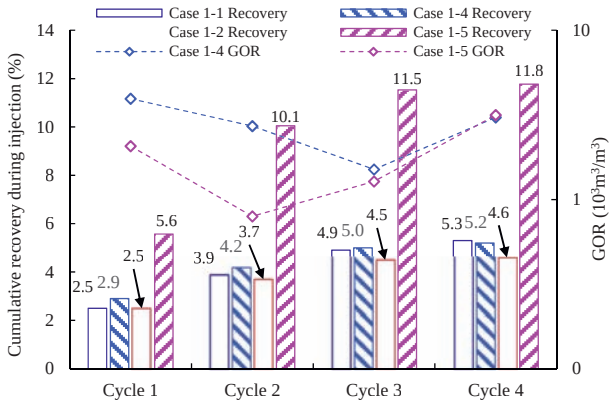


Fig. 9. The cumulative oil recovery and the gas-oil ratio in the injection stage at varying injection timings with cycles.

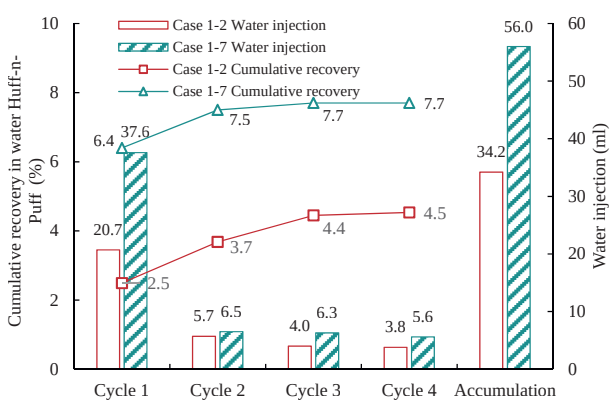


Fig. 10. The variation of cumulative recovery and water injection with cycles in different water injection volumes and injection stages in fractured-vuggy cores.

cumulative oil recovery, along with a more rapid attainment of oil-water equilibrium.

4.2.3. Effect of fractured-vuggy filling on single well unit water huff-n-puff

Water huff-*n*-puff experiments were conducted on both filled and unfilled cores after depletion to 1.2 Pb (cases 1-1 and 1–3). The difference in recovery was minimal, with cumulative values of 5.3% and 5.9%, respectively. In case 1–4 and case 1–6, water injection experiments were performed on both filled and unfilled cores after depletion below the bubble pressure. At the end of the depletion stage, the gas-oil ratios within the cores were identical, and the oil properties were essentially the same, indicating that the oil and gas phases had reached an equilibrium state.

Throughout each round of water injection and subsequent production, the filled core exhibited a uniform degassing delay phenomenon when the pressure was below the bubble pressure. This delay resulted in consistently higher oil recovery in the filled core compared to the unfilled core throughout the water huff-*n*-puff process. The maximum oil recovery observed in the filled core was 11.9%, which represents an increase of 6.7% over that of the unfilled core, as detailed in Fig. 11. This analysis demonstrates that the presence of filling materials within the cores can significantly impact oil recovery, especially during production below the bubble pressure. The observed degassing delay in the filled cores enhances the efficacy of the water injection process, resulting in improved oil recovery compared to unfilled cores.

4.3. Multi-well unit water injection development mood and mechanism

After natural energy depletion, the water injection development of multi-well units can be divided into two stages: continuous water flooding and asynchronous water flooding. In continuous flooding, injected water restores reservoir pressure and displaces oil through gravity segregation. However, once water breakthrough occurs, the water cut rises rapidly, especially in fault-fractured-vuggy reservoirs where fractures and caves create dominant flow channels. Asynchronous injection–production helps mitigate this channeling by redistributing flow paths, thereby improving sweep efficiency and enhancing oil recovery.

4.3.1. Effect of injection timing on multi-well unit water injection development

Table 7 presents the results of experiments for case 2-2 and case 2–3, which involve filled multiple fractured-vuggy core subjected to natural energy depletion at pressures of 1.2 Pb and 0.5 Pb, respectively. These cases utilize bottom injection and top production methods to enable continuous water flooding and asynchronous injection-production experiments. The cumulative oil recovery for the filled multiple fractured-vuggy core following depletion to both 1.2 Pb and 0.5 Pb was recorded at 11.9% and 35.8%, respectively.

During continuous water flooding, water breakthrough occurred after injecting 0.88 HCPV at 1.2 Pb, giving an oil recovery of 58.7%. At 0.5 Pb, breakthrough occurred earlier at 0.55 HCPV, with recovery of 36.7% (Figs. 12 and 13). The lower reservoir pressure in case 3, which was below the bubble pressure, resulted in an increase in the viscosity and density of the remaining oil following the natural energy depletion stage. This increase in viscosity contributes to higher viscous resistance. Moreover, when water was injected from the bottom of the core, significant microscopic fingering was observed, which caused rapid water channeling and a reduced degree of oil-water displacement. Consequently, this led to an earlier water breakthrough and a shorter period of water-free production.

Conversely, when water injection occurs above the bubble pressure, the oil remains undegassed. Due to gravitational segregation, a larger volume of water can be injected before water breakthrough takes place, resulting in an extended period of water-free production and improved oil recovery. This underscores the critical importance of the timing of water injection in relation to bubble pressure, as it significantly affects the efficiency of oil recovery in multi-well units. Notably, injections performed above the bubble pressure have demonstrated superior results.

In the context of the continuous water flooding process, the oil production rates observed in case 2-2 and case 2–3 were comparable prior to the water breakthrough. However, following the water breakthrough, the water cut increased rapidly, leading to a significant decline in the oil production rate to a negligible level. At this juncture, the injected water primarily moved vertically, driving the oil in a “piston-like” manner along the vertical direction. Most of the oil recovery during the water flooding process occurred during the water-free production phase. After the

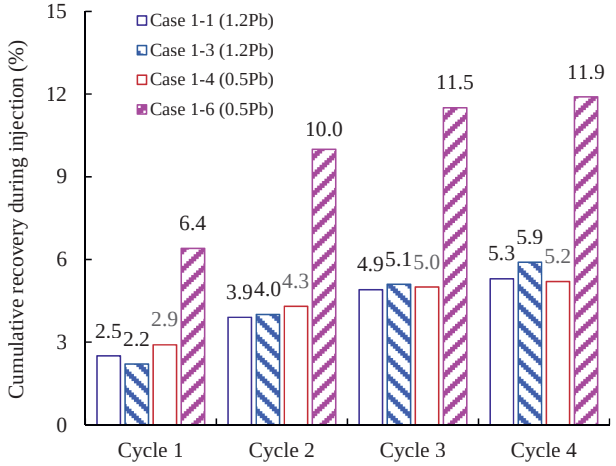


Fig. 11. Variation of cumulative recovery during the injection stages within different cycles.

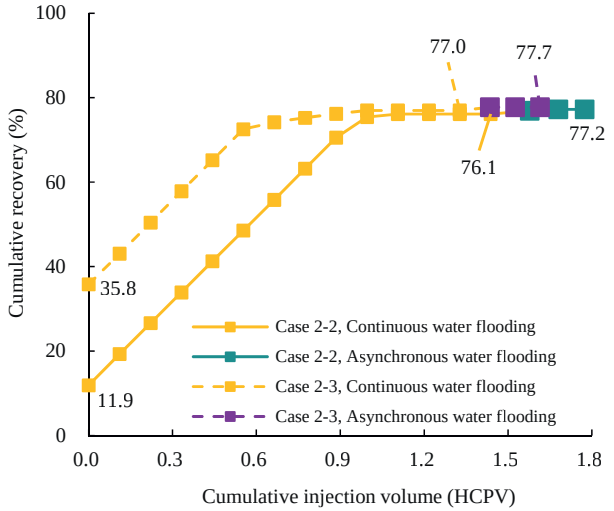


Fig. 12. Variation of cumulative recovery with cumulative injection volumes during the injection phase.

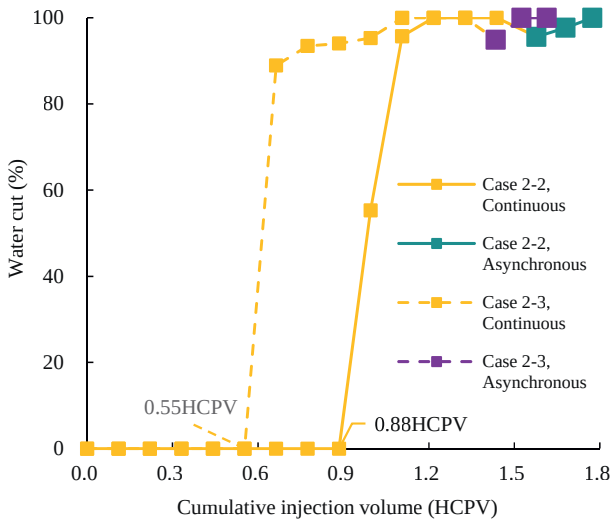


Fig. 13. Variation of water cut with the cumulative injection volume.

continuous water flooding phase ended, the cumulative water injection volumes for the two cases exhibited a discrepancy of only 0.1 HCPV, with cumulative oil recoveries of 76.1% and 77.0%, respectively.

The cumulative oil recovery following the continuous water flooding phase was found to be nearly identical, irrespective of whether the reservoir was depleted below or above the bubble pressure. In terms of water cut changes, the adoption of a continuous water flooding strategy, which includes deep injection and shallow production, after depleting the reservoir above the bubble pressure, allows for an extended period of water-free production. However, from an economic perspective, it is advisable to deplete the reservoir below the bubble pressure before initiating the continuous water flooding procedure of “deep injection and shallow production".

This strategy optimizes the economic efficiency of oil extraction by leveraging the increased viscosity and density of oil present below the bubble pressure to enhance oil recovery during the continuous water flooding phase. Furthermore, it capitalizes on an extended water-free production period enabled by gravity segregation when injecting above the bubble pressure.

During the asynchronous injection-production stage, a distinct alternation between water injection and oil production is observed. Throughout the various stages of water injection and soaking within the core, the injected water generates a pressure pulse effect on the formation. This effect causes the redistribution of oil and water within the pores, fractures, and caves, resulting in a reduction of the water cut within the core. As illustrated in Fig. 13, the initial water cut exhibited reductions of 4.4% and 5.1% during the asynchronous injection-production stage in case 2-2 and case 2–3, respectively.

Following the reopening of the well for production, the combined effects of capillary pressure and differential displacement pressure facilitate the migration of oil from low-permeability matrix pores into high-permeability fractures and caves. This process expands the sweep volume of the injected water, thereby enhancing oil recovery. However, the influence of asynchronous injection production on oil recovery is limited, with the majority of its effect occurring during the initial two cycles, as illustrated in Fig. 12. This limitation can be attributed to two primary factors: first, the conclusion of the continuous water flooding stage, the cumulative oil recovery had already exceeded 76%, leaving only a modest quantity of residual oil in the core. Second, during the asynchronous injection-production stage, the reservoir pressure experienced a slight increase from 1.5 Pb (54 MPa) to 1.8 Pb (65 MPa). The limited volume of injected water resulted in a comparatively low oil-water displacement efficiency, which in turn led to minimal additional oil recovery during this stage.

4.3.2. Impact of injection location on multi-well unit water injection development

Table 7 compares the effects of injection location after depletion to 1.2 Pb in filled multiple fractured-vuggy cores (cases 2-2 and 2–4). At the end of the natural energy depletion stage, the cumulative oil recovery was approximately equivalent for both cases, at 11.8%. Following depletion, water injection was initiated from both the bottom and top of the core, with the pressure increased to 1.5 Pb to begin continuous water flooding. In case 2-2 (deep injection and shallow production), water breakthrough occurred after injecting 0.88 HCPV, resulting in an oil recovery of 64.3%. In contrast, in case 2–4 (shallow injection and shallow production), water breakthrough occurred after injecting 0.22 HCPV, yielding an oil recovery of 20.1%.

By the end of the waterflooding stage, the cumulative oil recovery for the deep injection, shallow production method (case 2-2) reached 76.1%, compared to 31.9% for the shallow injection, shallow production method (case 2–4). The deep injection, shallow production approach achieved an oil recovery that was 44.2% higher than that of the shallow injection, shallow production method (see Figs. 14 and 15).

This significant difference highlights the critical role of injection location in improving recovery rates in fractured-vuggy reservoirs, particularly within multi-well units where strategic injection and production practices can substantially improve oil recovery.

The impact of gravity during the water flooding process is based on the displacement method employed. When water is injected from the bottom and moves upward, gravitational separation driven by the density difference between oil and water results in a relatively stable waterfront. In this context, gravity plays a positive and predominant role, with the displacement mechanism resembling a “piston-like” action. This configuration not only enhances oil displacement efficiency but also prolongs the period of water-free production and increases overall oil recovery.

Conversely, when water is injected from the top of the core, the initial oil recovery performance resembles that of the deep

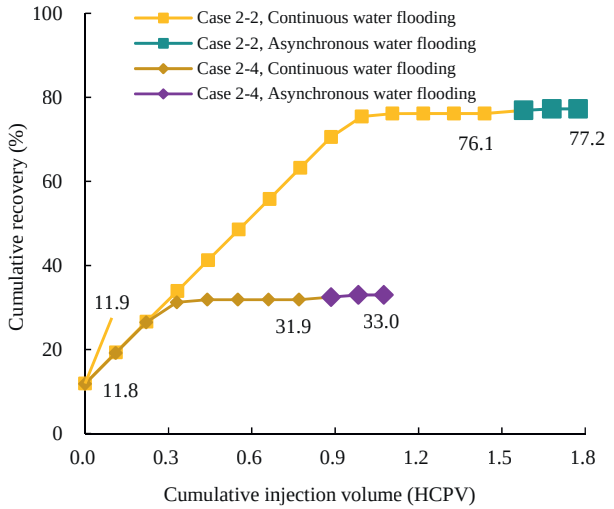


Fig. 14. Variation of the degree of water-driven recovery with cumulative injected HCPV during the injection phase.

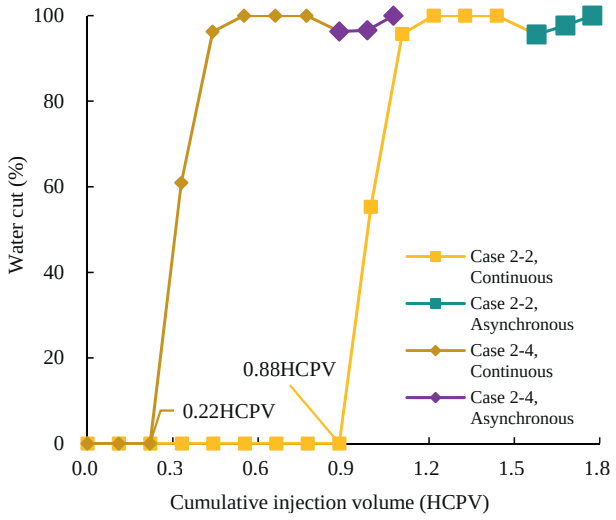


Fig. 15. Variation of water content with cumulative injection volume.

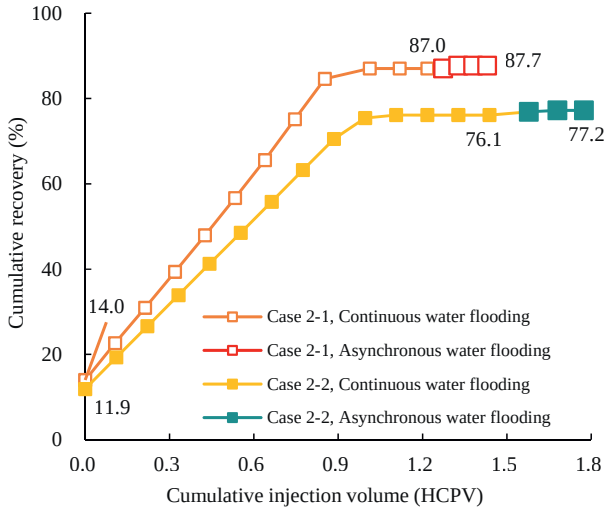


Fig. 16. Variation of cumulative oil recovery with cumulative injected volume during water injection phase.

injection, shallow production method. However, the influence of gravity induces vertical convection and channeling phenomena, which results in the rapid descent of the injected water and subsequent early water breakthroughs. This occurrence reduces the efficiency of oil displacement, ultimately leading to a reduction in overall oil recovery.

The experimental results indicate that a deep injection and shallow production well pattern combined with piston-like displacement can significantly extend the water-free production period while enhancing oil recovery. This approach effectively utilizes gravity to sustain a more controlled and efficient displacement front, thereby reducing water channeling and maximizing oil extraction from the reservoir.

4.3.3. Impact of fractured-vuggy filling on multi-well unit water injection development

Case 2-1 and case 2-2 involve experiments conducted on multiple fractured-vuggy cores to assess the impacts of continuous water flooding and asynchronous injection production above the bubble pressure. The unfilled multiple fractured-vuggy core

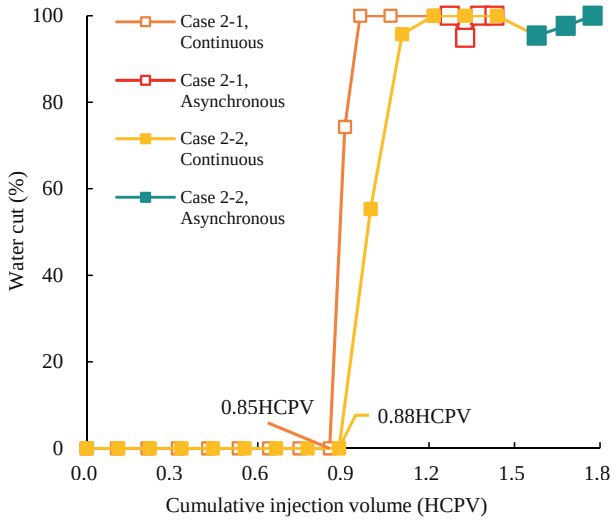


Fig. 17. Variation of water content with cumulative injection volume at injection stage.

exhibits superior reservoir characteristics, allowing gravity to play a dominant role during water flooding, which enhances higher displacement efficiency. In contrast, the filled core exhibits a significant reduction in porosity and permeability, resulting in increased flow resistance for the fluids.

At the point of water breakthrough, the volume of water injected into both core types was comparable. However, following the water breakthrough, the water cut in the filled core increased at a slower rate, indicating a lower oil displacement efficiency (see Figs. 16 and 17). By the end of the continuous water flooding stage, the cumulative water injection volumes for the unfilled and filled cores were 1.27 HCPV and 1.58 HCPV, respectively, with corresponding oil recoveries of 73.1% and 64.3%. This presents an 8.8% higher recovery for the unfilled core.

During the asynchronous injection-production stage, the contribution to oil recovery was limited, with an observed increase of approximately 1% in both cases. The final cumulative oil recovery rates were 87.4% for the unfilled core and 77.9% for the filled core.

This comparison highlights the significant impact of fractured-vuggy filling on the efficiency of water flooding in multi-well units. The reduced porosity and permeability in filled cores lead to increased resistance and decreased oil recovery efficiency. Conversely, unfilled cores, characterized by enhanced connectivity and reduced resistance, achieve higher overall oil recovery, particularly during the continuous waterflooding stage.

5. Conclusions

This study establishes a core model based on the cross-sectional profiles of fault-fractured-vuggy reservoirs, which are characterized by comparable porosity, fractures, and caves. Physical simulation experiments on water flooding in these reservoirs are conducted with the primary focus on developing water injection strategies for the FM fault-fractured-vuggy volatile oil reservoir. The aim is to provide guidance for enhancing oil recovery in such reservoirs.

The water injection development method for fault-fractured-vuggy volatile oil reservoirs is influenced by several factors. For single-well unit water huff-*n*-puff development, it is recommended that the reservoir be depleted to a pressure below the

bubble pressure by opening the deeper parts of the fractures. This strategy capitalizes on the elastic gas drive generated by the secondary gas cap formed through oil degassing. Subsequently, a large-volume water huff-*n*-puff approach with shallow injection and shallow production should be employed, increasing the water injection pressure to 1.5 Pb. This strategy takes advantage of gravity segregation, which arises from the density difference between oil and water. Continuous oil displacement can improve the oil recovery rate by over 5%. Natural energy depletion can achieve an oil recovery rate exceeding 67%, with the final cumulative recovery rate surpassing 72% after the water huff-*n*-puff process.

In fault-fractured-vuggy reservoirs with multi-well units, it is advisable to initially deplete the reservoir to below the bubble point pressure. This strategy utilizes gravity segregation, which capitalizes on the density differences between oil and water. By continuously flooding water from the bottom of the core while simultaneously producing oil from the top, the injected water functions as a "piston" that drives the oil vertically. This method leads to delayed water breakthrough, extends the period of water-free production, and enhances overall oil recovery. After deep injection and shallow production during continuous water flooding, recovery rates can exceed 75%. However, it is important to note that the asynchronous injection-production stage contributes only an additional 1% to the overall recovery.

Filled cores exhibit different dynamics compared to unfilled fractured-vuggy cores. When water injection development occurs above the bubble pressure after natural energy depletion, oil recovery is primarily influenced by the connectivity and physical properties of the reservoirs. Conversely, when depletion is conducted below the bubble pressure, the delayed degassing of oil, a non-equilibrium phenomenon, significantly enhances the impact of the reservoir's fluid properties on oil recovery.

CRediT authorship contribution statement

Hanmin Tu: Writing – review & editing, Writing – original draft, Methodology. **Jinchuan Wu:** Writing – review & editing, Writing – original draft, Data curation. **Zhouhua Wang:** Writing – original draft, Project administration, Methodology. **Xingliang Deng:** Resources, Funding acquisition. **Ping Guo:** Project administration, Methodology. **Zhiliang Liu:** Resources, Funding acquisition. **Haoqi Liao:** Writing – original draft, Data curation.

Declaration of competing interest

Here we confirm that there is no conflict of interest.

Acknowledgments

This work was supported by China National Petroleum Corporation's Top Ten Science and Technology Engineering Project (2022KT0603), China National Petroleum Corporation Major Science and Technology Project: Research on the Scaled Reserve Increase and Production and Exploration and Development Technology of Marine Carbonate Oil and Gas (No. 2023ZZ16); Research on the Efficient Development and Improved Recovery of Ultra-deep Fault-controlled Marine Carbonate Reservoirs (No. 2023ZZ16YJ02).

References

Chen, L., Jia, C., Zhang, R., Yue, P., Jiang, X., Wang, J., Su, Z., Xiao, Y., Lv, Y., 2024. High-pressure capacity expansion and water injection mechanism and indicator curve model for fractured-vuggy carbonate reservoirs. Petroleum 10 (3), 511–519.

Ding, Z., Wang, R., Chen, F., Yang, J., Zhu, Z., Yang, Z., Sun, X., Xian, B., Li, E., Shi, T., Zuo, C., Li, Y., 2020. Origin, hydrocarbon accumulation and oil-gas enrichment of fault-karst carbonate reservoirs: a case study of Ordovician carbonate reservoirs in South Tahe area of Halahatang oilfield, Tarim Basin. Petrol. Explor. Dev. 47 (2), 306–317.

Farhadi, H., Ayatollahi, S., Fatemi, M., 2022. Impact of rock morphology on the dominating enhanced oil recovery mechanisms by low salinity water flooding in carbonate rocks. Fuel 324, 124769.

Guo, W., Fu, S., Li, A., Xie, H., Cui, S., Nangendo, J., 2022. Experimental research on the mechanisms of improving water flooding in fractured-vuggy reservoirs. J. Pet. Sci. Eng. 213, 110383.

Guo, W., Huang, Z., Li, A., An, G., Cui, S., 2023. Visual experiments of bottom water and multi-well water and gas injection flooding for fault-controlled fractured-vuggy reservoirs. Phys. Fluids 35 (8), 083319.

Guo, Y., Liang, Y., Li, J., Gong, B., 2019. A novel connectivity-based hierarchical model for multi-scale fracture system in carbonate reservoir simulation. Fuel 250, 327–338.

He, J., Li, A., Wu, S., Tang, R., Lv, D., Li, Y., Li, X., 2020. Experimental investigation on injection and production pattern in fractured-vuggy carbonate reservoirs. Energies 13 (3), 603.

He, X., Wang, R., Yang, J., Li, S., Yao, C., Wu, G., 2022. Optimization of oil productivity from the ultra-depth strike-slip fault-controlled carbonate reservoirs in Northwestern China. Energies 15 (9), 3472.

Hou, J., Zheng, Z., Song, Z., Luo, M., Li, H., Zhang, L., Yuan, D., 2016. Three-dimensional physical simulation and optimization of water injection of a multi-well fractured-vuggy unit. Pet. Sci. 13 (2), 259–271.

Hu, J., Yang, S., Wang, B., Deng, H., Wang, M., Li, J., Zhao, S., Shen, B., Gao, X., Yang, K., 2024. Effect of pore structure characteristics on gas-water seepage behaviour in deep carbonate gas reservoirs. Geoenergy Sci. Eng. 238, 212881.

Jia, Z., Cheng, L., Wang, P., Wang, S., Jia, P., 2020. A practical methodology for production data analysis in carbonate reservoirs using new decline type curves. Geofluids 2020, 1873236.

Li, Q., Du, X., Tang, Q., Xu, Y., Li, P., Lu, D., 2021. A novel well test model for fractured vuggy carbonate reservoirs with the vertical bead-on-a-string structure. J. Pet. Sci. Eng. 196, 107938.

Lu, G., Zhang, L., Liu, Q., Xu, Q., Zhao, Y., Li, X., Deng, G., Wang, Y., 2022. Experiment analysis of remaining oil distribution and potential tapping for fractured-vuggy reservoir. J. Pet. Sci. Eng. 208, 109544.

Lu, Z., Ping, H., Chen, H., Zhang, Y., Xie, Z., Zhang, Y., Chen, Z., Yang, X., Zhang, X., Yang, K., Li, X., 2024. Geochemical characteristics of Ordovician crude oils in the FI17 strike-slip fault zone of the Fuman oilfield, Tarim basin: implications for ultra-deep hydrocarbon accumulation in the Tarim basin. Mar. Petrol. Geol. 163, 106800.

Ma, Q., Duan, T., 2023. Multi-level ultra-deep fault-controlled karst reservoirs characterization methods for the Shunbei field. Front. Earth Sci. 11, 1149678.

Ma, X., Li, H., Luo, H., Nie, S., Gao, S., Zhang, Q., Yuan, F., Ai, W., 2022a. Research on well selection method for high-pressure water injection in fractured-vuggy carbonate reservoirs in Tahe oilfield. J. Pet. Sci. Eng. 214, 110477.

Ma, Y., Cai, X., Yun, L., Li, Z., Li, H., Deng, S., Zhao, P., 2022b. Practice and theoretical and technical progress in exploration and development of Shunbei ultra-deep carbonate oil and gas field, Tarim Basin, NW China. Petrol. Explor. Dev. 49 (1), 1–20.

Qu, M., Hou, J., Wen, Y., Liang, T., 2020. Nitrogen gas channeling characteristics in fracture-vuggy carbonate reservoirs. J. Pet. Sci. Eng. 186, 106723.

Saw, R.K., Mandal, A., 2023. Experimental investigation on fluid/fluid and rock/fluid interactions in enhanced oil recovery by low salinity water flooding for carbonate reservoirs. Fuel 352, 129156.

Shen, A., Hu, A., Qiao, Z., Zheng, J., She, M., Pan, L., 2024. Development and preservation mechanism of deep and ultra-deep carbonate reservoirs. Sci. China Earth Sci. 67 (11), 3367–3385.

Tian, F., Di, Q., Jin, Q., Cheng, F., Zhang, W., Lin, L., Wang, Y., Yang, D., Niu, C., Li, Y., 2019. Multiscale geological-geophysical characterization of the epigenic origin and deeply buried paleokarst system in Tahe Oilfield, Tarim Basin. Mar. Petrol. Geol. 102, 16–32.

Wang, D., Li, Y., Hu, Y., Li, B., Deng, X., Liu, Z., 2016. Integrated dynamic evaluation of depletion-drive performance in naturally fractured-vuggy carbonate reservoirs using DPSO-FCM clustering. Fuel 181, 996–1010.

Wang, J., Liu, H., Xu, J., Zhang, H., 2012. Formation mechanism and distribution law of remaining oil in fracture-cavity reservoir. Petrol. Explor. Dev. 39 (5), 624–629.

Wang, J., Liu, H., Ning, Z., Zhang, H., Hong, C., 2014. Experiments on water flooding in fractured-vuggy cells in fractured-vuggy reservoirs. Petrol. Explor. Dev. 41 (1), 74–81.

Wang, Q., 2023. Origin of gas condensate reservoir in Fuman Oilfield, Tarim Basin, NW China. Petrol. Explor. Dev. 50 (6), 1295–1307.

Wang, S., Liu, H., Deng, X., Zhu, Y., Zhang, Y., Zhao, S., Su, Y., 2023. Genetic mechanism of multiphase states of Ordovician oil and gas reservoirs in Fuman oilfield, Tarim Basin, China. Mar. Petrol. Geol. 157, 106449.

Wang, Y., Hou, J., Tang, Y., Song, Z., 2019. Effect of vug filling on oil-displacement efficiency in carbonate fractured-vuggy reservoir by natural bottom-water drive: a conceptual model experiment. J. Pet. Sci. Eng. 174, 1113–1126.

Wen, Y., Hou, J., Xiao, X., Li, C., Qu, M., Zhao, Y., Zhong, W., Liang, T., Wu, W., 2023. Utilization mechanism of foam flooding and distribution situation of residual

oil in fractured-vuggy carbonate reservoirs. Pet. Sci. 20 (3), 1620–1639.
Wu, L., Wang, P., Zhang, C., Feng, X., Qian, Z., Zhou, L., 2023. Long-lived paleo-uplift controls on Neoproterozoic-Cambrian black shales in the Tarim basin. Mar. Petrol. Geol. 155, 106343.
Yang, W., Zhang, D., Lei, G., 2020. Experimental study on multiphase flow in fracture-vug medium using 3D printing technology and visualization techniques. J. Pet. Sci. Eng. 193, 107394.
Yang, X., Wang, R., Deng, X., Li, S., Zhang, H., Yao, C., 2022. Theoretical exploration of water injection gravity flooding oil in ultra-deep fault-controlled fractured-cavity carbonate reservoirs. Petrol. Explor. Dev. 49 (1), 133–143.
Zhang, S., Huang, H., Su, J., Liu, M., 2015. Ultra-deep liquid hydrocarbon exploration potential in cratonic region of the Tarim Basin inferred from gas condensate genesis. Fuel 160, 583–595.
Zhang, Y., Lin, C., Ren, L., Sun, C., Li, J., Zhao, X., Wu, M., 2025. Multi-scale characterization of reservoir space features in yueman area of Fuman Oilfield in Tarim Basin. Processes 13 (2), 310.
Zhao, Y., Lu, G., Zhang, L., Yang, K., Li, X., Luo, J., 2020. Physical simulation of waterflooding development in large-scale fractured-vuggy reservoir considering filling characteristics. J. Pet. Sci. Eng. 191, 107328.
Zhu, B., Tang, H., Yin, S., Chen, G., Zhao, F., Li, L., 2022a. Experimental and numerical investigations of particle plugging in fracture-vuggy reservoir: a case study. J. Pet. Sci. Eng. 208, 109610.
Zhu, G., Li, J., Zhang, Z., Wang, M., Xue, N., He, T., Zhao, K., 2020. Stability and cracking threshold depth of crude oil in 8000 m ultra-deep reservoir in the Tarim Basin. Fuel 282, 118777.
Zhu, Y., Zhang, Y., Zhao, X., Xie, Z., Wu, G., Li, T., Yang, S., Kang, P., 2022b. The fault effects on the oil migration in the ultra-deep fuman oilfield of the Tarim Basin, NW China. Energies 15 (16), 5789.
Zou, W., Gu, Y., 2024. Solvent exsolution and liberation from different heavy oil-solvent systems in bulk phases and porous media: a comparison study. Energies 17 (10), 2287.